Chemical Engineering Journal 420 (2021) 129642

Contents lists available at ScienceDirect

Chemical Engineering Journal

journal homepage: www.elsevier.com/locate/cej

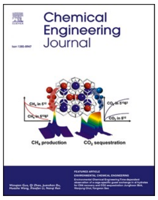

Localizing concentrated electrolyte in pore geometry for highly reversible aqueous Zn metal batteries

Run Xiao [a,b,1], Zhao Cai [a,1], Renming Zhan [a], Jindi Wang [a], Yangtao Ou [a], Zhu Yuan [a], Li Wang [c], Ziheng Lu [d], Yongming Sun [a,*]

[a] *Wuhan National Laboratory for Optoelectronics, Huazhong University of Science and Technology, Wuhan 430074, China*
[b] *China-EU Institute for Clean and Renewable Energy, Huazhong University of Science and Technology, Wuhan 430074, China*
[c] *Institute of Nuclear & New Energy Technology, Tsinghua University, Beijing 100084, China*
[d] *Department of Materials Science and Metallurgy, University of Cambridge, Cambridge CB3 0FS, United Kingdom*

ARTICLE INFO

Keywords:
Rechargeable aqueous batteries
Zn metal anode
Nanoporous structure
Locally concentrated electrolyte
Electrochemical reversibility

ABSTRACT

Rechargeable aqueous Zn metal batteries are promising for large-scale renewable energy storage. However, the aqueous Zn metal battery chemistry encounters severe irreversibility issues, as manifested by the non-uniform metallic Zn plating and undesired side-reactions of corrosion. Herein, we report a highly-reversible aqueous Zn metal anode with accurately controlled nanopore structure, by which the space charge distribution could be regulated and interface-localized concentrated electrolyte was enabled. Consequently, the nanoporous Zn (npZn) electrode exhibited high electrochemical reversibility for 750 h under the measurement with a combination of electrochemically Zn stripping/plating cycling (1 mA cm^{-2} and 1 mAh cm^{-2} for 25 cycles) and resting (50 h), and looping. Moreover, a npZn||$NaVO_3$ cell exhibited a high capacity of 200 mAh g^{-1} and a long lifespan with considerable capacity retention (76% for 1500 cycles), and high reversibility (Coulombic efficiency of 99.8%), which was more stable than the counterpart with pristine Zn anode (short-circuit after 600 cycles).

1. Introduction

The unprecedented energy crisis and environment degradation have brought extensive research attention to energy storage technologies with enhanced environmental friendliness and reduced price[1–10], of which rechargeable aqueous zinc metal batteries (RAZMBs) stand out due to the following advantages: First, Zn metal possesses a high theoretical capacity as a anode (820 mAh g^{-1}), which helps to achieve high energy batteries[11–14]; Second, Zn metal is abundant and environmentally benign, beneficial for low cost and large scale application; Third, aqueous electrolytes, particularly the mild $ZnSO_4$ electrolytes developed in recent years, are intrinsically safe and compatible with Zn metal anodes, and thus can enable high battery safety. [15–17]. Nevertheless, Zn metal anodes suffer from detrimental drawbacks including non-uniform electrochemical plating and inevitable side-reactions of corrosion, resulting in its poor electrochemical performance, which constitute the bottlenecks for scale-up utilization of RAZMBs[18–20]. Therefore, it is urgent to develop highly reversible Zn metal anodes for practical RAZMBs with long lifespan.

In pursuit of high-performance Zn metal anodes for RAZMBs, various strategies including surface protection[21,22], nanostructure design [23,24], and electrolyte optimization[25] have been proposed to stabilize metallic Zn during electrochemical cycling. In particular, concentrated or "water-in-salt" electrolytes became one of the most important strategies by increasing the availability of Zn^{2+} ions, decreasing the content of free water[26,27]. Recently, Wang[28] and Ji [29] adopted concentrated "water-in-salt" electrolytes (1 M $Zn(TFSI)_2$ + 20 M LiTFSI and $ZnCl_2$, respectively) and realized highly reversible Zn metal anodes. Despite these exciting advancements, the issues of high cost, high viscosity, and low ionic conductivity for concentrated electrolytes have not yet been solved [30,31]. The essence of concentrated electrolyte is to tune the solvation structure of Zn^{2+} ions and changes the electrochemical behaviors at the metal/electrolyte interface. In this study, we proposed that locally concentrated electrolyte at the metal/electrolyte interface could retain the advantages of concentrated electrolyte, and greatly reduce the cost and viscosity of the electrolyte and increase the overall ionic conductivity at the same time in comparison to the concentrated electrolytes, therefore being ideal for aqueous Zn metal

---

* Corresponding author at: Wuhan National Laboratory for Optoelectronics, Huazhong University of Science and Technology, Wuhan 430074, China.
E-mail address: yongmingsun@hust.edu.cn (Y. Sun).

[1] These authors contributed equally to this work.

https://doi.org/10.1016/j.cej.2021.129642
Received 19 February 2021; Received in revised form 21 March 2021; Accepted 30 March 2021

anode, especially three-dimensional (3D) Zn electrode with large surface area that suffered from severe side-reactions of corrosion.

In this work, we enabled interface-localized concentrated electrolyte at a 3D nanoporous Zn (npZn) metal electrode by designated use of the space charge effect in the accurately controlled nanopore structure, as confirmed by both theoretical simulation and spectroscopic studies. The npZn electrode with interface-localized concentrated electrolyte showed uniform Zn plating behavior and suppressed side reactions simultaneously. As a consequence, the npZn electrode exhibited high electrochemical reversibility for 750 h under the measurement with a combination of electrochemically Zn stripping/plating cycling (1 mA cm^{-2} and 1 mAh cm^{-2}, 25 cycles) and resting (50 h), and looping. In contrast, the pristine Zn electrode failed after 30 h of cycling under the same test condition. Moreover, a npZn||NaVO$_3$ full cell showed a high capacity of 200 mAh g^{-1} and a long lifespan with considerable capacity retention (76% for 1500 cycles), which outperformed the pristine Zn||NaVO$_3$ full cell (failed after 600 cycles due to short-circuit). These results suggested a promising route for the stabilization of Zn metal anode in rechargeable aqueous batteries.

2. Results and discussion

Fig. 1a illustrates electrochemical plating behavior of a conventional Zn metal foil (pristine Zn) electrode in ZnSO$_4$ electrolyte, where inhomogeneous plating and chemical corrosion of metallic Zn take place. In the case of concentrated electrolyte (Fig. 1b), uniform Zn plating can be achieved due to the increased availability of Zn^{2+} ions, meanwhile chemical corrosion can be suppressed because of the less content of free water. However, the concentrated electrolyte suffers from high cost, high viscosity and low ionic conductivity, which is detrimental to the practical application. Compared to the above two situations, a 3D nanoporous Zn metal electrode with interface-localized concentrated electrolyte can be an ideal case for low-cost and highly-reversible Zn metal electrode (Fig. 1c). The space charge effect of nanoporous metal provides the platform for regulating the charge density in electric double layer on the electrode surface to achieve interface-localized concentrated electrolyte, while the bulk of the electrolyte remains unchanged. To investigate the space charge distribution of a nanoporous Zn metal electrode in ZnSO$_4$ electrolyte, finite element simulations were employed to understand the relationship between the ion/charge concentration and the pore diameter. The electric potential and the ion (e.g. Zn^{2+}, Zn (H$_2$O)$_6^{2+}$, SO$_4^{2-}$) concentration at the Zn metal|ZnSO$_4$

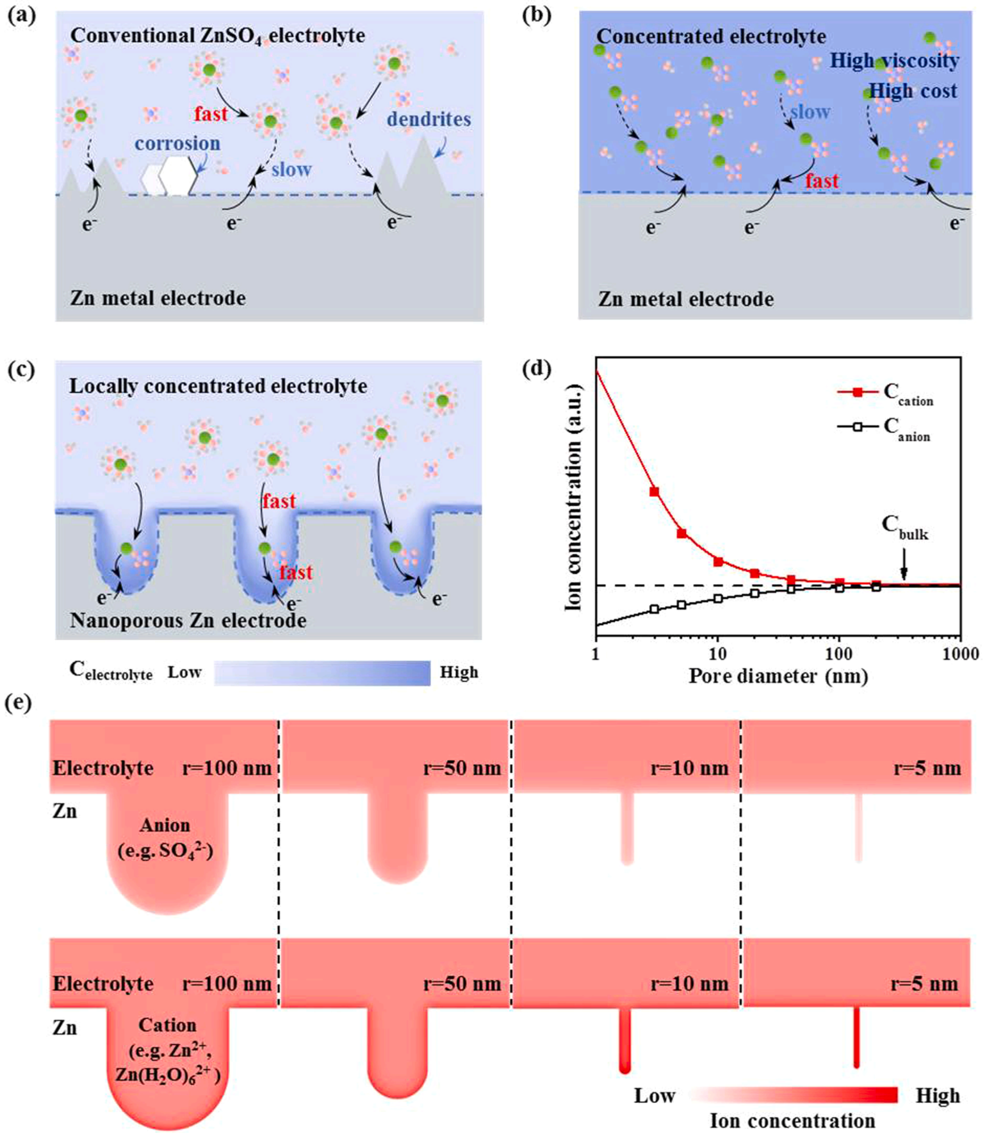

Fig. 1. Schematic illustration of Zn plating processes on (a) Zn metal electrode with conventional ZnSO$_4$ electrolyte, (b) Zn metal electrode with concentrated electrolyte, and (c) nanoporous Zn electrode with interface-localized concentrated electrolyte. (d) The ion concentration at the electric double layer of nanoporous Zn metal with different pore diameters based on Poisson-Nernst-Planck equations. (e) Surface charge densities of the cations and anions at the interface of ZnSO$_4$ electrolyte and nanoporous Zn metal with different pore diameters ranging from 5 nm to 100 nm.

electrolyte interface were modeled following the Gouy-Chapman-Stern double layer model (Fig. S1), the space charge effect on the effective ion concentration of electrolyte within the pores became significant with the shrinkage of the pore sizes, as shown in Fig. 1d. In fact, with the decrease of pore sizes (e.g. < 40 nm), the surface of Zn metal became cation-rich, demonstrating the high Zn^{2+} ion concentration. For clarity, the ion concentration at the interface of $ZnSO_4$ electrolyte and Zn metal pores with diameters ranging from 100 nm to 5 nm were shown in Fig. 1e. It was found that the cations including Zn^{2+} and $Zn(H_2O)^{2+}$ in the double layer at the metal/electrolyte interfaces became enriched with decreased nanopore size (especially 10 and 5 nm). Such results revealed the fact that interface-localized concentrated electrolyte can in principle be achieved within a nanoporous Zn metal with a pore size ranging from 1 to 40 nm.

Inspired by the above theoretical findings, we propose an alloying-dealloying method to prepare npZn electrode with controlled pore size (Fig. 2a). The pristine Zn foil showed a relatively flat surface with a silver-white metallic lustre, as confirmed by scanning electron microscope (SEM) and optical microscopy (OM) images (Fig. S2). After the alloying reaction with Li metal at room temperature, Li-Zn alloy layer formed on the surface of the Zn metal and Li-Zn/Zn composite foil was produced, as indicated by the result of X-ray Diffraction (XRD, Fig. S3). The Li-Zn/Zn composite foil was then dealloyed using ethanol immersion to produce a Zn electrode with 3D nanoporous structure (noted as npZn). The OM image suggested that the surface of npZn electrode became dull after dealloying (Fig. 2b). SEM images showed the hierarchical pore structures of the as-prepared npZn electrode, mainly including submicronmeter-sized macropores with average pore diameter of ~500 nm and mesopores with average pore diameter of ~20 nm (Fig. 2c), and the thickness of the nanoporous layer was ~15 μm (Fig. 2d). It was noted that the pore size and the thickness of the nanoporous layer could be finely tuned by changing the temperature for the alloying reaction. When an elevated temperature of 100 °C was applied for the alloying reaction, the average pore diameters of the mesopores increased to ~80 nm, the thickness of the nanoporous layer also increased to ~28 μm (Fig. S4). When the alloying reaction temperature was further increased to 200 °C (>180 °C, the melting point of Li metal), the nanoporous layer even punctured the entire Zn foil (~145 μm, Fig. S5). To confirm the space charge effect in the npZn electrode, energy-dispersive X-ray spectroscopy (EDS) analysis was employed. As shown in Fig. 3c, the npZn electrode after immersing in $ZnSO_4$ electrolyte and washed with deionized water for 5 min showed a clear elemental mapping of S, suggesting that $ZnSO_4$ was confined in the nanopores and could not be washed out. Moreover, the electrode after

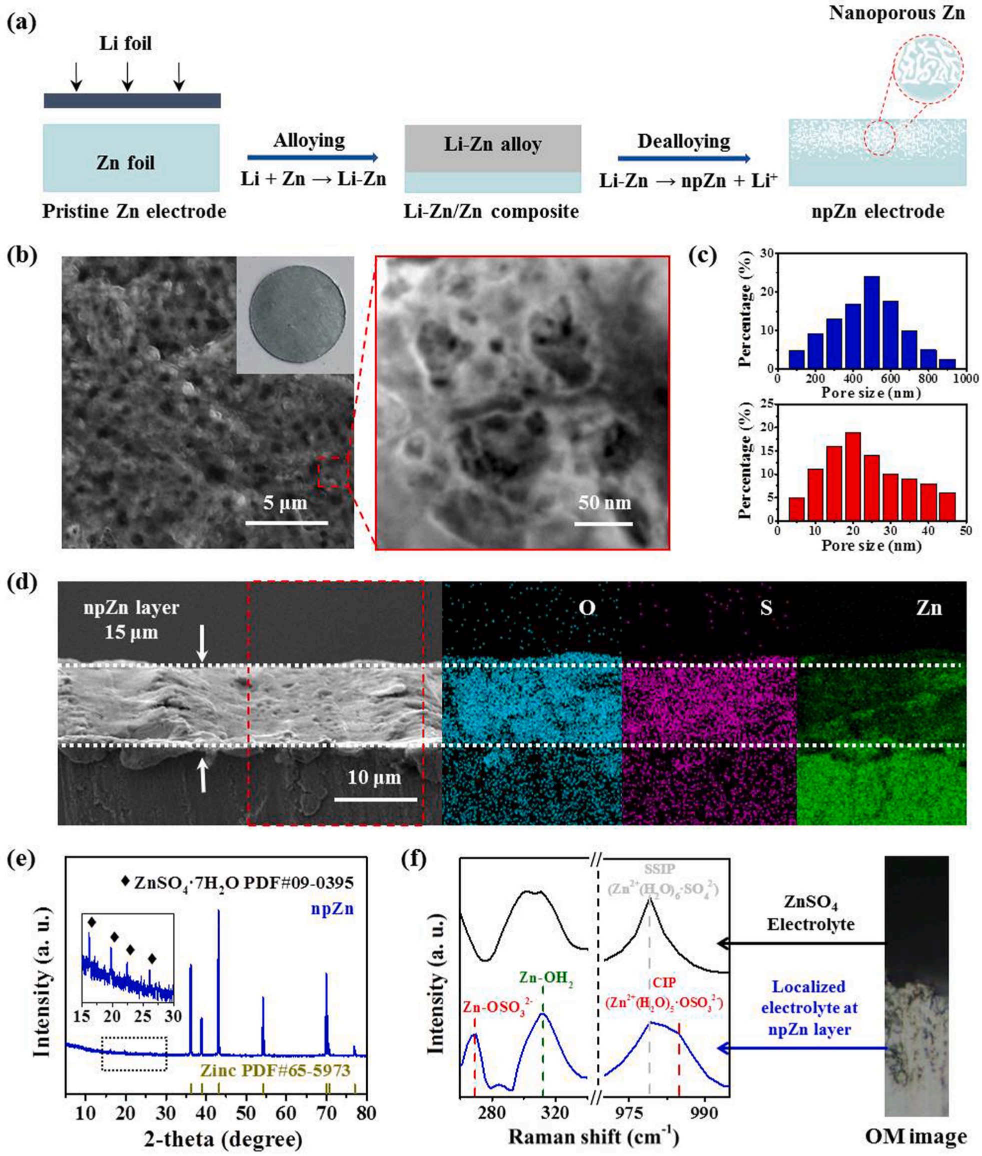

Fig. 2. (a) Schematic illustration of the preparation of npZn electrode. (b) Top-view SEM image of the npZn electrode. The inset showed the digital picture of the as-prepared npZn electrode. (c) Size distribution of the macropores and mesopores of the npZn electrode. (d) Cross-section SEM and EDS elemental mapping images and (e) XRD pattern of the npZn electrode after immersing in $ZnSO_4$ eletrolyte and washed with deionized water for 5 min. (f) Raman analysis of the $ZnSO_4$ electrolyte configuration in and outside the 3D nanoporous channels of the npZn electrode.

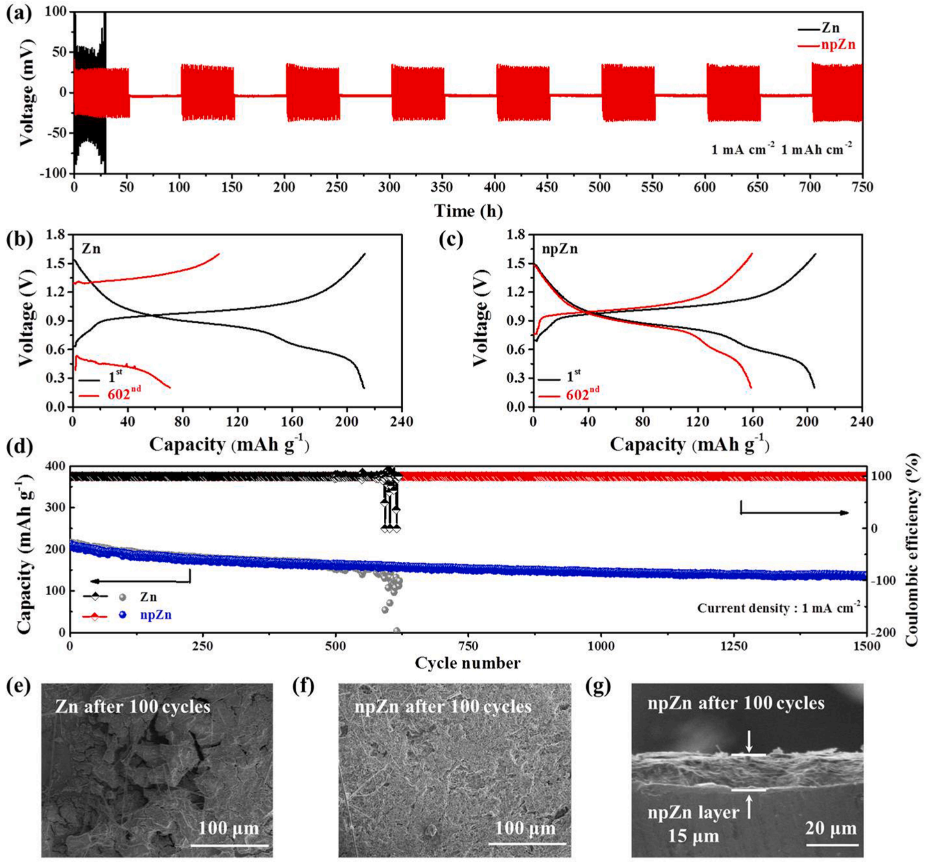

Fig. 3. (a) Voltage profiles of the pristine Zn and npZn electrode under dynamic measurement with a combination of electrochemical cycling (1 mA cm^{-2} and 1 mAh cm^{-2}, 25 cycles) and resting (50 h), and looping. Galvanostatic charge/discharge curves of (b) pristine Zn||$NaVO_3$ and (c) npZn||$NaVO_3$ cells at the 1st cycle and the 602nd cycle. (d) Cycling performance of pristine Zn||$NaVO_3$ and npZn||$NaVO_3$ cells at a current density of 1 mA cm^{-2}. (e) Top-view SEM image of the pristine Zn electrode after 100 cycles at 1 mA cm^{-2} and 1 mAh cm^{-2}. (f) Top-view and (g) cross-section SEM images of the npZn electrode after 100 cycles at 1 mA cm^{-2} and 1 mAh cm^{-2}.

immersion and washing was dried under vacuum and examined by XRD. As shown in Fig. 2e, the XRD peaks for $ZnSO_4{\cdot}7H_2O$ further confirmed the confined $ZnSO_4$ within the npZn electrode in the electrolyte, indicating the concentrated electrolyte in the nanopores that can hardly be washed out. To get direct evidence of the electrolyte configuration in the metallic pores and verify the locally concentrated electrolyte, Raman spectroscopy was employed to investigate the ion coordination forms in $ZnSO_4$ electrolyte (e.g. $Zn^{2+}(H_2O)_6^{2+}{\cdot}OSO_3^{2-}$ and $Zn^{2+}{\cdot}OSO_3^{2-}$). A npZn electrode with $ZnSO_4$ electrolyte was examined with a Raman laser focused on the bulk $ZnSO_4$ electrolyte or the local electrolyte at the npZn layer. As demonstrated in Fig. 2f, only the Zn-OH_2 vibration at 310 cm^{-1} was observed in the saturated $ZnSO_4$ electrolyte (~3.3 M) above the surface of the npZn/$ZnSO_4$ electrode[32–35]. Under the same test condition, the Zn-O vibration of $[Zn^{2+}{\cdot}OSO_3^{2-}]$ ligand mode (270 cm^{-1}) appeared in the electrolyte in the nanoporous layer of the npZn/$ZnSO_4$ electrode[32–35], suggesting a great degree of ion-association, which often appeared when the ions were more crowded. Furthermore, the contact ion pair (CIP. i.e. $[Zn^{2+}(H_2O)_5{\cdot}OSO_3^{2-}]$), was observed in the electrolyte in the nanoporous layer, suggesting a high association degree of Zn^{2+} and SO_4^{2-} that existed only in high-concentration electrolytes in previous reports[32–35]. In contrast, the saturated $ZnSO_4$ electrolyte showed only the solvent separated ion pair (SSIP, i.e. $[Zn^{2+}(H_2O)_6{\cdot}SO_4^{2-}]$)[32–35], and thus indicated the less free water in the nanoporous Zn layer of npZn according to the Eigen-Tamm mechanism. As a comparison, the npZn electrode alloying at 100 °C with an average pore size above 40 nm did not get Raman signal of $[Zn^{2+}{\cdot}OSO_3^{2-}]$ ligand and CIP mode (Fig. S6), which was in consist with the theoretical prediction, and in turn further confirmed the localized concentrated electrolyte at npZn electrode with controlled nanopore size.

The npZn electrode with 3D nanoporous structure would show enlarged electrochemical surface area (ESA) and enhanced charge transfer, both of which are favorable for improving the electrochemical performance of an electrode. The ESA of the electrodes, indicated by the electrical double-layer capacitance (C_{eff}), were calculated by fitting the EIS results (Fig. S7, S8), and the results are shown in Table S1. The C_{eff} of the pZn electrode was 74 times that of the pristine Zn, suggesting a much higher surface area for the npZn electrode. Moreover, the npZn electrode exhibited a much smaller charge transfer resistance (54.7 Ω) than the pristine Zn electrode (289.8 Ω, Fig. S7). To evaluate the electrochemical performance of the Zn metal electrode, Zn||Zn symmetric cells were assembled using aqueous $ZnSO_4$ electrolyte. In consideration of the practical application scenarios where batteries are intermittently used but not continuously cycling, we performed dynamic measurement with a combination of electrochemical stripping/plating cycling (1 mA cm^{-2} and 1 mAh cm^{-2}, 25 cycles) and resting (50 h), and looping. As a result, the npZn electrode exhibited stable electrochemical cycling for 750 h with a low overpotential of 25 mV. As a contrast, the pristine Zn electrode showed a short cycle life of ~30 h with a much larger overpotential of 60 mV (Fig. 3a). We noted that the npZn electrode exhibited advancement in overpotential when comparing with most of the Zn metal electrodes in recent publications (Table S2). With the increasing current density and areal capacity (2 mA cm^{-2} and 2 mAh cm^{-2}, Fig. S9), the npZn electrode also showed excellent cycling stability with a low overpotential of 36 mV for 150 h, outperforming the pristine Zn (200 mV, 16 h). The excellent electrochemical performance of the npZn electrode was also verified in cells paired with $NaVO_3$ cathode. The as-prepared $NaVO_3$ cathode material showed a nanobelt morphology with size of ~2 μm in length and ~150 nm in width (Fig. S10). Cycled at a current density of 600 mA g^{-1} (corresponding to an areal capacity of 0.35 mAh cm^{-2}), both the pristine Zn||$NaVO_3$ and npZn||$NaVO_3$ cells showed a high initial capacity of 200 mAh g^{-1}. The pristine Zn||$NaVO_3$ cell failed after 602 cycles due to short-circuit, while the npZn||$NaVO_3$ cell displayed a much more stable cycling performance, which delivered

~80% of its initial discharge capacity at the 602nd cycle (Fig. 3b and 3c). Moreover, the npZn||$NaVO_3$ cell achieved a long lifespan (>1500 cycles) with considerable capacity retention (76%), and high reversibility (Coulombic efficiency of 99.8%). The improved electrochemical reversibility of the npZn electrode was contributed to the pomoted uniform plating and suppressed chemical corrosion of metallic Zn. As shown in Fig. S11, non-uniform Zn deposits were observed for the pristine Zn electrode after plating 1 mAh cm^{-2} of Zn at 1 mA cm^{-2}. For the npZn electrode, the plated Zn was relatively uniform after the same Zn plating process. Moreover, after 100 cycles at 1 mA cm^{-2} and 1 mAh cm^{-2}, a large number of randomly stacked Zn deposits were observed for the pristine Zn electrode (Fig. 3e, S12), which would further cause metallic dendrites and eventually battery failure. The overall structure and morphology of the npZn electrode was well maintained after 100 plating/stripping cycles (Fig. 3f, 3 g), demonstrating a stable electrode structure during cycling. As to the chemical corrosion, the pristine Zn electrode exhibited a low corrosion potential of −0.983 V with a large corrosion current density of 6.9 mA cm^{-2}. The npZn electrode showed a high corrosion potential of −0.975 V and a low corrosion current density of 4.0 mA cm^{-2} (Fig. S13), suggesting markedly suppressed side reactions. The differernt corrosion behaviors of the pristine Zn and npZn electrode in $ZnSO_4$ electrolyte were also verified by XRD and SEM. The pristine Zn electrode produced a large amount of corrosion products after resting in aqueous $ZnSO_4$ electrolyte for 7 d, as evidenced by the significant diffraction of layered zinc hydroxide sulfate (ZHS) in XRD (Fig. S14) and sheet-like products in SEM (Fig. S15a, S15c). As a contrast, the npZn electrode showed much weaker diffraction signals of ZHS corrosion products (Fig. S14) and much less sheet-like ZHS corrosion products under the same test conditions (Fig. S15b, S15d). Moreover, we noted that no new phase such as ZHS was formed for the npZn electrode after 100 cycles at 1 mA cm^{-2} and 1 mAh cm^{-2} (Fig. S16). These results were well consistent with the improved electrochemical reversibility of the npZn electrode and provided a new option in achieving advanced Zn metal anodes for practical RAZMBs with long lifespan.

3. Conclusion

In this work, we reported a Zn metal anode with well-tailored nanopore structure enabling locally concentrated electrolyte for highly reversible RAZMBs. The interface-localized concentrated electrolyte formed *via* the space charge effect within the precisely regulated nanopore structure, which simultaneously promoted the uniform plating of Zn and suppressed the side reactions of chemical corrosion. The as-achieved npZn electrode exhibited a high electrochemical reversibility for 750 h under dynamic measurement with a combination of electrochemically Zn stripping/plating cycling at (1 mA cm^{-2} and 1 mAh cm^{-2}, 25 cycles) and resting (50 h), and looping. The highly reversible npZn electrode also enabled an essentially stable npZn||$NaVO_3$ cells. The design of nanoporous electrode with locally concentrated electrolyte demonstrated in this study provides a new strategy for developing highly reversible Zn metal anodes for RAZMBs towards sustainable energy storage.

Declaration of Competing Interest

Acknowledgements

Y.S. acknowledges the financial support by the Innovation Fund of Wuhan National Laboratory for Optoelectronics of Huazhong University of Science and Technology. Z.C. thanks the China Postdoctoral Science Foundation (No. 2018M640694, 2020T130223). The authors would like to thank the Analytical and Testing Center of Huazhong University of Science and Technology as well as the Center for Nanoscale Characterization & Devices of Wuhan National Laboratory for Optoelectronics for providing the facilities to conduct the characterization. The authors also thank Mr. William Orbell at University of Oxford for helpful discussion.

Appendix A. Supplementary data

Supplementary data to this article can be found online at https://doi.org/10.1016/j.cej.2021.129642.

References

[1] Y. Liang, H. Dong, D. Aurbach, Y. Yao, Current status and future directions of multivalent metal-ion batteries, Nat. Energy 5 (9) (2020) 646–656.

[2] J. Zheng, Q. Zhao, T. Tang, J. Yin, C.D. Quilty, G.D. Renderos, X. Liu, Y. Deng, L. Wang, D.C. Bock, C. Jaye, D. Zhang, E.S. Takeuchi, K.J. Takeuchi, A. C. Marschilok, L.A. Archer, Reversible epitaxial electrodeposition of metals in battery anodes, Science 366 (6465) (2019) 645–648.

[3] X. Fan, B. Liu, J. Liu, J. Ding, X. Han, Y. Deng, X. Lv, Y. Xie, B. Chen, W. Hu, C. Zhong, Battery technologies for grid-level large-scale electrical energy storage, Trans. Tianjin Univ. 26 (2) (2020) 92–103.

[4] M. Xu, L. Fei, W. Zhang, T. Li, W. Lu, N. Zhang, Y. Lai, Z. Zhang, J. Fang, K. Zhang, J. Li, H. Huang, Tailoring anisotropic Li-ion transport tunnels on orthogonally arranged Li-rich layered oxide nanoplates toward high-performance Li-ion batteries, Nano Lett. 17 (3) (2017) 1670–1677.

[5] L. Chen, Z. Yang, Y. Huang, Monoclinic VO2 (D) hollow nanospheres with super-long cycle life for aqueous zinc ion batteries, Nanoscale 11 (27) (2019) 13032–13039.

[6] Y. Zhang, Q. Su, W. Xu, G. Cao, Y. Wang, A. Pan, S. Liang, A confined replacement synthesis of bismuth nanodots in MOF derived carbon arrays as binder-free anodes for sodium-ion batteries, Adv. Sci. 6 (2019) 1900162.

[7] Q. Wang, Z. Zhang, M. Wang, F. Liu, L. Jiang, B.o. Hong, J. Li, Y. Lai, Bioinspired fiber-like porous Cu/N/C electrocatalyst facilitating electron transportation toward oxygen reaction for metal-air batteries, Nanoscale 10 (33) (2018) 15819–15825.

[8] Y. Cai, G. Fang, J. Zhou, S. Liu, Z. Luo, A. Pan, G. Cao, S. Liang, Metal-organic framework-derived porous shuttle-like vanadium oxides for sodium-ion battery application, Nano Res. 11 (1) (2018) 449–463.

[9] Y. Jing, B. Liu, X. Zhu, F. Ouyang, J. Sun, Y. Zhou, Tunable electronic structure of two-dimensional transition metal chalcogenides for optoelectronic applications, Nanophotonics 9 (2020) 1675–1694.

[10] P. Li, Q. Xie, L. Zheng, G. Feng, Y. Li, Z. Cai, Y. Bi, Y. Li, Y. Kuang, X. Sun, X. Duan, Topotactic reduction of layered double hydroxides for atomically thick two-dimensional non-noble-metal alloy, Nano Res. 10 (9) (2017) 2988–2997.

[11] T.-H. Wu, Y. Zhang, Z.D. Althouse, N. Liu, Nanoscale design of zinc anodes for high-energy aqueous rechargeable batteries, Mater. Today Nano 6 (2019), 100032.

[12] Z. Zhao, J. Zhao, Z. Hu, J. Li, J. Li, Y. Zhang, C. Wang, G. Cui, Issues and opportunities facing aqueous zinc-ion batteries, Energy Environ. Sci. 12 (2019) 1938–1949.

[13] Z. Wang, J. Huang, Z. Guo, X. Dong, Y. Liu, Y. Wang, Y. Xia, A metal-organic framework host for highly reversible dendrite-free zinc metal anodes, Joule 3 (5) (2019) 1289–1300.

[14] Z. Zhao, X. Fan, J. Ding, W. Hu, C. Zhong, J. Lu, Challenges in zinc electrodes for alkaline zinc-air batteries: Obstacles to commercialization, ACS Energy Lett. 4 (9) (2019) 2259–2270.

[15] X. Zeng, J. Hao, Z. Wang, J. Mao, Z. Guo, Recent progress and perspectives on aqueous Zn-based rechargeable batteries with mild aqueous electrolytes, Energy Storage Mater. 20 (2019) 410–437.

[16] M. Song, H. Tan, D. Chao, H.J. Fan, Recent advances in aqueous zinc-ion batteries, Adv. Funct. Mater. 1802564 (2018).

[17] B. Tang, L. Shan, S. Liang, J. Zhou, Issues and opportunities facing aqueous zinc-ion batteries, Energy Environ. Sci. 12 (11) (2019) 3288–3304.

[18] H. Li, L. Ma, C. Han, Z. Wang, Z. Liu, Z. Tang, C. Zhi, Advanced rechargeable zinc-based batteries: recent progress and future perspectives, Nano Energy 62 (2019) 550–587.

[19] L. Kang, M. Cui, F. Jiang, Y. Gao, H. Luo, J. Liu, W. Liang, C. Zhi, Nanoporous $CaCO_3$ coatings enabled uniform Zn stripping/plating for long-life zinc rechargeable aqueous batteries, Adv. Energy Mater. 8 (2018) 1801090.

[20] Q. Yang, Q. Li, Z. Liu, D. Wang, Y. Guo, X. Li, Y. Tang, H. Li, B. Dong, C. Zhi, Dendrites in Zn-based batteries, Adv. Mater. 32 (2020) 2001854.

[21] Z. Cai, Y. Ou, J. Wang, R. Xiao, L. Fu, Z. Yuan, R. Zhan, Y. Sun, Chemically resistant Cu-Zn/Zn composite anode for long cycling aqueous batteries, Energy Storage Mater. 27 (2020) 205–211.

[22] Y. Zhang, G. Wang, F. Yu, G. Xu, Z. Li, M. Zhu, Z. Yue, M. Wu, H.-K. Liu, S.-X. Dou, C. Wu, Chao Wu. Highly reversible and dendrite-free Zn electrodeposition enabled by a thin metallic interfacial layer in aqueous batteries, Chem. Eng. J. (2020) 128062, https://doi.org/10.1016/j.cej.2020.128062.

[23] J. Wang, Z. Cai, R. Xiao, Y. Ou, R. Zhan, Z. Yuan, Y. Sun, A chemically polished zinc metal electrode with a ridge-like structure for cycle-stable aqueous batteries, ACS Appl. Mater. Interfaces 12 (20) (2020) 23028–23034.

[24] S.-B. Wang, Q. Ran, R.-Q. Yao, H. Shi, Z. Wen, M. Zhao, X.-Y. Lang, Q. Jiang, Lamella-nanostructured eutectic zinc–aluminum alloys as reversible and dendrite-free anodes for aqueous rechargeable batteries, Nat. Commun. 11 (2020) 1634.

[25] J. Zhao, J. Zhang, W. Yang, B. Chen, Z. Zhao, H. Qiu, S. Dong, X. Zhou, G. Cui, L. Chen, "Water-in-deep eutectic solvent" electrolytes enable zinc metal anodes for rechargeable aqueous batteries, Nano Energy 59 (2019) 625–634.

[26] L. Yu, S. Chen, H. Lee, L. Zhang, M.H. Engelhard, Q. Li, S. Jiao, J. Liu, W. Xu, J.-G. Zhang, A localized high-concentration electrolyte with optimized solvents and lithium difluoro (oxalate) borate additive for stable lithium metal batteries, ACS Energy Lett. 3 (2018) 2059–2067.

[27] D. Chao, S.-Z. Qiao, Toward high-voltage aqueous batteries: super-or low-concentrated electrolyte? Joule 4 (2020) 1846–1851.

[28] F. Wang, O. Borodin, T. Gao, X. Fan, W. Sun, F. Han, A. Faraone, J.A. Dura, K. Xu, C. Wang, Highly reversible zinc metal anode for aqueous batteries, Nat. Mater. 17 (2018) 543–549.

[29] C. Zhang, J. Holoubek, X. Wu, A. Daniyar, L. Zhu, C. Chen, D.P. Leonard, I. A. Rodríguez-Pérez, J.-X. Jiang, C. Fang, X. Ji, A $ZnCl_2$ water-in-salt electrolyte for a reversible Zn metal anode, Chem. Commun. 54 (100) (2018) 14097–14099.

[30] X. Ren, S. Chen, H. Lee, D. Mei, M.H. Engelhard, S.D. Burton, W. Zhao, J. Zheng, Q. Li, M.S. Ding, M. Schroeder, J. Alvarado, K. Xu, Y.S. Meng, J. Liu, J.-G. Zhang, W.u. Xu, Localized high-concentration sulfone electrolytes for high-efficiency lithium-metal batteries, Chem 4 (8) (2018) 1877–1892.

[31] L. Qin, N. Xiao, J. Zheng, Y.u. Lei, D. Zhai, Y. Wu, Localized high-concentration electrolytes boost potassium storage in high-loading graphite, Adv. Energy Mater. 9 (44) (2019) 1902618, https://doi.org/10.1002/aenm.v9.4410.1002/aenm.201902618.

[32] W.W. Rudolph, M.H. Brooker, P.R. Tremaine, Raman spectroscopy of aqueous $ZnSO_4$ solutions under hydrothermal conditions: solubility, hydrolysis, and sulfate ion pairing, J. Solution Chem. 28 (1999) 621–630.

[33] W.W. Rudolph, C.C. Pye, Zinc(II) hydration in aqueous solution. A Raman spectroscopic investigation and an ab-initio molecular orbital study, Phys. Chem. Chem. Phys. 1 (19) (1999) 4583–4593.

[34] P. Kruus, A.C. Hayes, W.A. Adams, Determination of ratios of sulfate to bisulfate ions in aqueous solutions by Raman spectroscopy, J. Solution Chem. 14 (1985) 117–128.

[35] H. Yang, Y. Qiao, Z. Chang, H. Deng, P. He, H. Zhou, A metal-organic framework as a multifunctional ionic sieve membrane for long-life aqueous zinc-iodide batteries, Adv. Mater. 32 (2020) 2004240.